https://doi.org/10.5194/angeo-2023-6
Preprint. Discussion started: 28 February 2023

Annales Geophysicae Discussions
Open Access
EGU

Relativistic Kinematic Effects in the Interaction Time of Whistler-Mode Chorus Waves and Electrons in the Outer Radiation Belt

Livia R. Alves[1], Márcio E.S. Alves[2,*], Ligia A. da Silva[1,3], Vinicius Deggeroni[1], Paulo R. Jauer[1,3], and David G. Sibeck[4]

[1]National Institute for Space Research (INPE), Sao Jose dos Campos-SP-Brazil
[2]Universidade Estadual Paulista (UNESP), Instituto de Ciência e Tecnologia, São José dos Campos, SP, 12247-004, Brazil
[*]Also at Universidade Estadual Paulista (UNESP), Faculdade de Engenharia e Ciências de Guaratinguetá, Departamento de Física e Química, Guaratinguetá, SP, 12516-410, Brazil.
[3]State Key Laboratory of Space Weather, National Space Science Center, Chinese Academy of Sciences
[4]NASA Goddard Space Flight Center, Greenbelt, MD, USA

Correspondence: Livia Alves (livia.alves@inpe.br)

Abstract. Whistler-mode chorus waves propagate outside the plasmasphere. As they interact with energetic electrons in the outer radiation belt electrons, the phase space density distribution can change due to energy or pitch angle diffusion. Calculating the wave-particle interaction time is crucial to estimate the particle's energy or pitch angle change efficiently. Although the wave and particle velocities are a fraction of the speed of light, in calculating the interaction time, the special relativistic effects are often misleading, incomplete, or simply unconsidered. In this work, we derive an equation for the wave-particle interaction time considering the special relativity kinematic effect. We solve the equation considering typical magnetospheric plasma parameters, and compare the results with the non-relativistic calculations. Besides, we apply the methodology and the equation to calculate the interaction time for one wave cycle in four case studies. We consider wave-particle resonance conditions for chorus waves propagating at any wave normal angle in a dispersive and cold plasma. We use Van Allen Probes for in situ measurements of the relevant wave parameters for the calculation, the ambient magnetic field, and energetic electron flux under quiet and disturbed geomagnetic conditions. Thus, we use a test particle approach to calculate the interaction time for parallel and oblique propagating waves. Also, we evaluate the variation of pitch angle scattering for relativistic electrons interacting with whistler-mode chorus waves propagating parallel to the ambient magnetic field. If the relativistic effects are not taken into account, the interaction time can be $\sim 30\%$ lower for quiet periods and a half lower for disturbed periods. As a consequence, the change in pitch angle is also underestimated. Besides, the longest interaction time occurs at wave-particle interaction with high pitch angle electrons, with energy $\sim 100's$ of keV, interacting with quasi-parallel propagating waves. Additionally, the change in pitch angle depends on the time of interaction, and similar discrepancies can be found when the time is calculated with no special relativity consideration. The results described here have several implications for modeling relativistic outer radiation belt electron flux resulting from the wave-particle interaction. Finally, since we considered only one wave-cycle interaction, the average result from some interactions can bring more confident results in the final flux modeling.

https://doi.org/10.5194/angeo-2023-6
Preprint. Discussion started: 28 February 2023

Annales Geophysicae Discussions
Open Access
EGU

1 Introduction

The inner magnetosphere's outer radiation belt is filled mainly with electrons in a broad energy range, from tens of keV to MeV, distributed in several pitch angles. In the equatorial region, the loss cone instability (for a detailed description, see Lakhina et al. (2010) and references therein) caused by the electron's source population (tens of eV to tens of keV) anisotropy, produce whistler-mode chorus waves (Tsurutani and Smith, 1974, 1977; Shprits et al., 2007, 2008; Lakhina et al., 2010; Lam et al., 2010; Tsurutani et al. , 2013). Chorus waves are very low frequency (VLF) (from hundreds of Hz to a few kHz) in whistler mode and propagate as discrete wave packets.

In the magnetosphere, the whistler-mode chorus waves can be observed either at low frequency, i.e., $0.1\Omega_{ce} < \omega < 0.5\Omega_{ce}$ (when the emission occurs in frequencies lower than half the electron gyrofrequency (Ω_{ce})) and high frequency ($0.5\Omega_{ce} < \omega < 0.9\Omega_{ce}$) (Artemyev et al., 2016). At the frequency $\omega = 0.5\Omega_{ce}$, chorus waves are likely to interact with low-energy electrons due to Landau resonance, which causes damping (Tsurutani and Smith, 1974; Bortnik et al. , 2006). The wave vector can be oriented quasi-parallel to the ambient magnetic field ($\theta \leq 45°$) when exhibiting right-handed circularly polarized emission (Artemyev et al., 2016), or oblique ($45° < \theta \leq 50°$), and very oblique ($\theta > 50°$) to the ambient magnetic field (Artemyev et al., 2016; Hsieh et al., 2020, 2022, and references therein). In the latter case, the electric field is elliptically polarized (Verkhoglyadova et al., 2010).

Chorus waves are observed outside the plasmasphere, mainly at the dawn side of the magnetosphere. Often, they interact with the electrons seed population (hundreds of keV) and accelerate them to MeV energies (Thorne et al., 2005; Tu et al., 2014; Santolik et al., 2009; Reeves et al., 2003; Reeves et al. , 2013; Jaynes et al. , 2015; Da Silva et al., 2021; Lejosne et al. , 2022; Hua et al. , 2022) or diffuse in pitch angle scattering (Horne and Thorne, 2003a; Horne et al., 2003b; Alves et al., 2016; Zhang et al., 2017; Liu et al., 2020; Guo et al., 2021), which may cause electrons to precipitate into the atmosphere. The wave-particle interaction succeeds when the resonance condition is satisfied, which implies a balance among the wave frequency, electron's energy, plasma density, and ambient magnetic field strength (ω_{pe}/Ω_e), as shown by Horne et al. (2003b).

The wave-particle interaction time (T_r) is a crucial parameter in estimating the energy and pitch angle diffusion coefficients since they are time-dependent processes (Walker, 1993; Lakhina et al., 2010; Tsurutani et al. , 2013; Hsieh et al., 2020, 2022). The ambient plasma parameters as density and magnetic field, besides wave group velocity and propagation direction, are applied in the estimate of T_r considering electrons' interacting with coherent whistler mode chorus waves. Besides, the direct equations of motion are considered. Regarding that both electrons and wave speed are a fraction of the speed of light, the special relativity theory must be applied to solve the kinematics of this problem. However, the relativistic approach is often simplified or misused.

In this work, we apply concepts from the special relativity theory to estimate the interaction time (T_r) between whistler-mode chorus waves propagating in a cold plasma magnetosphere (where group velocity is $0.3c$ to $0.5c$) and energetic electrons (with energy ~ 0.1 to 2 MeV). We consider that the resonance occurs in the electron's reference frame, while the result of such

https://doi.org/10.5194/angeo-2023-6
Preprint. Discussion started: 28 February 2023

Annales Geophysicae Discussions
Open Access
EGU

interaction and their parameters are measured in the local inertial reference frame of the satellite. Thus, we consider a complete kinematic relativistic description to obtain the information in the satellite frame. The interaction time is calculated using the test particle approach (Tsurutani and Smith, 1974; Lakhina et al., 2010; Horne et al., 2003b; Bortnik et al., 2008). We use the Van Allen Probes measurement of wave parameters, ambient magnetic field, density, electron fluxes, and equatorial pitch angle to apply the interaction time equation in the estimate of pitch angle scattering for four case studies with parallel propagating waves. Finally, we compare our results with the non-relativistic interaction time $T_{\rm nr}$.

2 Wave-particle interaction in the Radiation Belt

2.1 Group velocity for parallel and oblique propagation

The inner magnetosphere plasma density is a fundamental parameter to determine the wave dispersion relation (and group velocity) involved in the Doppler shift cyclotron resonance condition (see density implications to the resonant diffusion surfaces, e.g., Horne and Thorne, 2003a). Several works have shown that plasma density varies due to the magnetospheric activity under different solar wind drivers (e.g., see discussions at Li et al., 2014; Sicard-Piet et al., 2014; Allison et al., 2021), leading to an additional difficulty in imposing simplifications in the calculation of parameters related to the ambient electron plasma density. In this work, we are interested in the wave-particle interaction outside the plasmasphere, so we derive the dispersion relation from the solution of the Appleton-Hartree equation. Thus, the whistler-mode chorus wave group velocity in the magnetosphere is calculated by the solution of the dispersion relation $\eta(\omega) = kc/\omega$ in a cold plasma, neglecting ions contributions (Bittencourt, 2004)

$$\eta(\omega) = \left[1 - \frac{X(1-X)}{(1-X) - \frac{1}{2}Y^2\sin^2\theta + \sqrt{(\frac{1}{2}Y^2\sin^2\theta)^2 + (1-X)^2Y^2\cos^2\theta}}\right]^{1/2}, \tag{1}$$

where $X = \omega_{pe}^2/\omega^2$, $Y = \Omega_{ce}/\omega$, with ω_{pe} is the plasma frequency and θ is the wave normal angle (WNA). The WNA is defined as the angle between the wave vector $\boldsymbol{k}$ and the ambient magnetic field $\boldsymbol{B_0}$. The positive signal in the square root in the denominator is chosen because we consider the ordinary right circularly polarized (RCP) wave propagation mode (Helliwell, 1965). We take the derivative of Eq. (1) to evaluate the group velocity ($v_g \equiv d\omega/dk$) for a given whistler mode chorus wave propagating at a given angle, such that θ can be chosen among parallel, quasi-parallel and oblique classification, related to the ambient magnetic field in any plasma density

$$\frac{v_g}{c} = \frac{1}{\eta + \omega d\eta/d\omega}. \tag{2}$$

For whistler-mode chorus waves propagating outside plasmapause, where density can vary from ~ 1 to $\sim 20\,\mathrm{cm}^{-3}$, the usual high-dense plasma approximation (e.g., see Bittencourt, 2004; Artemyev et al., 2016) is often inconvenient under disturbed geomagnetic conditions. Thus, we solve Eq. (2) for low electron density conditions. The wave group velocity and the maximum wave propagation frequency are significantly lowered as the WNA becomes oblique, as shown in Figure 1 because the ambient refractive index is not isotropic.

https://doi.org/10.5194/angeo-2023-6
Preprint. Discussion started: 28 February 2023

Annales Geophysicae Discussions
Open Access
EGU

2.2 Wave-particle cyclotron resonance condition

The whistler-mode chorus waves are generated near the geomagnetic equator, where they are often observed propagating at frequency ω, parallel to the field lines (Tsurutani and Lakhina, 1997; Santolik et al., 2009; Lakhina et al., 2010). Also, oblique chorus waves are observed at high latitudes (Omura, Y. , 2021; Artemyev et al., 2016) and can resonantly interact with electrons elsewhere (Mourenas et al., 2015).

Electrons undergoing a bouncing motion parallel to the magnetic field lines see a relativistic Doppler shift in the wave frequency from its frame of observation

$$\omega - \boldsymbol{k}\cdot\boldsymbol{v}_e = n\frac{\Omega_{ce}}{\gamma(v_e)}, \tag{3}$$

where the vector $\boldsymbol{v}_e$ is the electron velocity and $\gamma(v_e) = (1 - v_e^2/c^2)^{-1/2}$. The resonant cyclotron harmonics are given by the integer number n, with $n = 0$ corresponding to the Landau resonance condition. The gyrofrequency low-order harmonics $n = \pm 1, 2, 3, 4, 5$ are often observed for oblique wave vector propagation (Artemyev et al., 2016; Orlova et al., 2012; Subbotin et al., 2010; Lorentzen et al., 2001). If they are positive, the resonance is said to be normal; otherwise, it is anomalous (Tsurutani and Lakhina, 1997). The pitch angle scattering and energy diffusion occur when whistler-mode chorus wave group velocity and the relativistic electron propagation velocity fulfill the resonance condition in Eq. (3) (Tsurutani and Lakhina, 1997; Shprits et al., 2008; Lakhina et al., 2010).

The scalar product in Eq. (3) is calculated for an electron resonant speed and wave propagating in a dispersive media with phase (group) velocity given by Eq. 1 (2). From Eq. (3), we can obtain the electron speed for which the resonant condition is fulfilled in terms of the wave and plasma parameters. We call this the resonant relativistic electron's speed

$$\frac{v_e}{c} = \frac{\eta\cos\theta + (n\Omega_{ce}/\omega)[\eta^2\cos^2\theta + (n^2{\Omega_{ce}}^2/\omega^2 - 1)]^{1/2}}{\eta^2\cos^2\theta + n^2{\Omega_{ce}}^2/\omega^2}. \tag{4}$$

In the above equation, $\eta(\omega)$ is any dispersion relation chosen according to the application. Here we consider the dispersion relation given by Eq. (1). The Van Allen Probes in situ measurements (ambient density, magnetic field) are used in Eq. (4) to calculate typical values of the resonant kinetic energy

$$K_{res} = \frac{mc^2}{\sqrt{1 - v_e^2/c^2}} - mc^2, \tag{5}$$

of electrons that resonantly interact with the wave frequency in a given plasma condition and wave propagation direction. As shown in Figure 2, we calculate K_{res} for the gyrofrequency harmonic $n = +3$, ambient magnetic field $B_0 = 150$ nT, and electron plasma density $n_e = 2.0\ \mathrm{cm}^{-3}$. From Eq. (4), we can obtain the equation presented by Summers et al. (2012) if we use their notation[1] $v_e = v_R + v_\perp$ and take $\theta = 0$.

Figure 2 shows that in the low-frequency range of whistler mode chorus waves, i.e., $\omega < 0.45\Omega_{ce}$, the resonant electron energy shown does not change significantly as the WNA changes from $\theta = 0°$ to $50°$. On the other hand, for the high-frequency range of whistler mode chorus waves ($0.55 \leq \omega \leq 0.90$), oblique ($\theta \sim 50°$) chorus waves interaction with 10's of keV electrons may be limited to ($\theta > 50°$), since the group velocity is limited at $\omega/\Omega_{ce} = 0.6$ (as shown in Figure 1).

[1] In our notation $v_R = v_{gc}$. For further details, see section 3.

https://doi.org/10.5194/angeo-2023-6
Preprint. Discussion started: 28 February 2023

Annales Geophysicae Discussions
Open Access
EGU

3 Relativistic interaction time

The wave-particle interaction holds as the resonance condition prevails; after that, the interaction is ended. Thus, the interaction time T can be defined as the time elapsed by the resonant electron passing through the wave subelement with duration τ (Hsieh et al., 2020; Lakhina et al., 2010). Alternatively, one can also define it as the time needed for the phase difference between the wave and particle to change by 1 rad (Tsurutani and Lakhina, 1997; Walker, 1993). In the following calculations, we consider the former definition.

In order to calculate the interaction time, one needs to define two reference frames to work on a relativistic kinematic scenario. The first one is the satellite frame (S) in which the measurement of the relevant physical quantities (including Tr) takes place, and the second one is the frame of the electron guiding center (S') in which the interaction occurs. Thus, the relative velocity between these two frames is the electron guiding center velocity $\boldsymbol{v}_{gc}$. The guiding center electron velocity is related to the electron's speed by the pitch angle α by the relation $v_{gc} = v_e \cos\alpha$. Since $\boldsymbol{v}_{gc}$ is parallel to the ambient magnetic field $\boldsymbol{B_0}$, the angle between $\boldsymbol{v}_{gc}$ and the wave vector coincides with the WNA given by θ. In S' the interaction time can be written as

$$T' = \frac{L'}{v'_g}, \tag{6}$$

where L' and v'_g are the wave subelement's scale size and the wave's group velocity in this same frame. If v_{gc} is much smaller than the speed of light, one can relate the group velocity in both frames v'_g and v_g simply by the vector addition formula of $\boldsymbol{v}_g$ and $\boldsymbol{v}_{gc}$. However, in the general case for which the electrons are relativistic, this is no longer true, and one needs to use the well-known relativistic formula of the addition of velocities. Therefore, we have

$$v'_g = \frac{\sqrt{v_g^2 + v_{gc}^2 - 2v_g v_{gc}\cos\theta - \left(\frac{v_g v_{gc}\sin\theta}{c}\right)^2}}{1 - \frac{v_g v_{gc}}{c^2}\cos\theta}, \tag{7}$$

where θ is the angle (in the S frame) between $\boldsymbol{v}_g$ and $\boldsymbol{v}_{gc}$.

Another relativistic effect to consider in the transition from one frame to another is the Lorentz-FitzGerald contraction. If L_0 is the scale size of the wave in its proper reference frame, in the S' frame, we have

$$L' = \frac{L_0}{\gamma(v'_g)}, \tag{8}$$

where the Lorentz factor is

$$\gamma(v'_g) = \frac{1}{\sqrt{1 - \frac{v'^2_g}{c^2}}}. \tag{9}$$

In the same fashion, the scale size of the wave in the S frame is

$$L = \frac{L_0}{\gamma(v_g)}, \tag{10}$$

https://doi.org/10.5194/angeo-2023-6
Preprint. Discussion started: 28 February 2023

Annales Geophysicae Discussions

and after combining the Eqs. (8) and (10) we obtain

$$L' = \frac{\gamma(v_g)}{\gamma(v'_g)} L. \tag{11}$$

Notice that if we have, for instance, $v'_g > v_g$, the subelement's wave scale size in the S' frame is smaller than the scale size measured in the satellite frame. The difference between the two sizes is more considerable as the electron's speed is higher.

Substituting the above equation in Eq. (6) we have

$$T' = \frac{\gamma(v_g)}{\gamma(v'_g)} \frac{L}{v'_g}. \tag{12}$$

Finally, the time dilation effect is the third relativistic kinematic effect. The interaction time in the S frame can be obtained from the above expression in the S' frame by multiplying the Eq. (12) by a new Lorentz factor $\gamma(v_{gc})$. The final equation is

$$T = \frac{\gamma(v_{gc})\gamma(v_g)}{\gamma(v'_g)} \frac{L}{v'_g}. \tag{13}$$

Therefore, if we use the Eq. (7) together with the Eq. (13), we obtain the expression of the interaction time with all quantities measured in the S frame. The final expression contemplates all the relativistic kinematic effects.

In Figure 3, we show the time of interaction calculated for different resonant energies and three different propagating WNA, i.e., parallel, $25°$ and $50°$, for an electron propagating with an $80°$ pitch angle (a) and a $25°$. The vertical lines indicate the wave-particle resonant interaction at $\sim 400, 840$, and 1500 Hz, respectively. These frequencies belong to the lower-band chorus waves, as shown in Figure 2. The interaction time shows a significant electron's pitch angle dependence and also with WNA, which is more relevant for the lowest energy electrons (kinetic energy ≤ 500 keV) corresponding to the seed particle population range that can be accelerated to the core energy. As the resonant electron energy increases, the time interaction time dependence on WNA decreases.

Additionally, a comparison of the time of interaction calculated through Eq. (13) with the time calculated without considering any relativistic correction is shown in Figure 4 for parallel propagating waves and $80°$ pitch angle electrons. According to our results, the non-relativistic time is under-estimated even for low-energy electrons. This happens due to the wave group velocity being very high in the magnetospheric density conditions. Thus the relativistic addition velocity should be considered whatever the resonant electron energy.

The influence of these three relativistic kinematic effects on the time of interaction can be analyzed by plotting each term in Eq. (13) as a function of the electron resonant energy or wave frequency (not shown). Regarding the contribution of each term, we obtain that the main contribution comes from the L/v'_g ratio, which differentiates from the non-relativistic equation by the relativistic velocity addition (v'_g). Moreover, the difference in time due to the γ factor is 20% for parallel wave propagation at any resonant electron energy. It becomes more significant at kinetic energy higher than 1 MeV and as long as the WNA deviates from parallel.

https://doi.org/10.5194/angeo-2023-6
Preprint. Discussion started: 28 February 2023

Annales Geophysicae Discussions
Open Access
EGU

4 Application to Change in the relativistic electron pitch angle for parallel wave propagation

The change in pitch angle can be calculated using the test-particle approach as done by Tsurutani and Lakhina (1997) and later on, Lakhina et al. (2010). Let us start with the Lorentz equation

$$\frac{d\boldsymbol{p}}{dt} = q_e\left(\boldsymbol{E} + \boldsymbol{v}_e \times \boldsymbol{B}\right), \tag{14}$$

where $\boldsymbol{B}$ is the sum of the wave magnetic field $\boldsymbol{B}_w$ and the ambient magnetic field $\boldsymbol{B}_0$, the wave electric field is $\boldsymbol{E} = (\omega/k)\boldsymbol{B}_w \times \hat{k}$, $q_e = -e$ and $\boldsymbol{p} = \gamma(v_e)m_e\boldsymbol{v}_e$ are the electron charge and momentum respectively. For the WNA, let us consider the simple case for which $\theta = 0$. Considering $\boldsymbol{B}_0$ in the $+z$ direction of a local Cartesian coordinate system associated with the S frame we have the following components of the Eq. (14)

$$\frac{dp_x}{dt} = q_e\left[\frac{\omega}{k}B_y + (v_yB_0 - v_zB_y)\right], \tag{15}$$

$$\frac{dp_y}{dt} = q_e\left[-\frac{\omega}{k}B_x - (v_xB_0 - v_zB_x)\right], \tag{16}$$

$$\frac{dp_z}{dt} = q_e(v_xB_y - v_yB_x). \tag{17}$$

The electron momentum can be written as $\boldsymbol{p} = \boldsymbol{p}_\perp + \boldsymbol{p}_\parallel$ where $\boldsymbol{p}_\perp \equiv p_x\hat{i} + p_y\hat{j}$ is the momentum orthogonal to the ambient magnetic field and $\boldsymbol{p}_\parallel \equiv p_z\hat{k}$ is parallel to it. Therefore, the pitch angle can be obtained from $\tan\alpha = p_\perp/p_\parallel$ and we obtain the following formula for a small change in α

$$\Delta\alpha = \frac{p_\parallel dp_\perp - p_\perp dp_\parallel}{p^2}. \tag{18}$$

Combining Eqs. (15), (16) and (17) with the above equation, it is straightforward to show that

$$\Delta\alpha = \frac{q_eB_w\sin\phi}{\gamma(v_e)m_e}\left(\frac{\omega}{k}\frac{\cos\alpha}{v_e} - 1\right)\Delta t, \tag{19}$$

where ϕ is the angle between the wave magnetic field and the orthogonal component of the electron momentum.

If we further consider that the resonant condition given by Eq. (3) is satisfied we finally obtain a fully relativistic equation for a small change in the pitch angle due to a wave-particle interaction

$$\Delta\alpha = \frac{\Omega_{ce}}{\gamma(v_e)}\frac{B_w}{B_0}\sin\phi\left[\frac{\omega\cos^2\alpha}{(n\Omega_{ce}/\gamma(v_e) - \omega)} + 1\right]T, \tag{20}$$

where we used the definition $\Omega_{ce} \equiv eB_0/m_e$ and $\Delta t = T$ is the time of interaction given by Eq. (13).

Previous works, e.g., Lakhina et al. (2010); Tsurutani and Lakhina (1997), estimate the change in pitch angle for non-relativistic electrons and chorus waves, both propagating parallel to the ambient magnetic field in a dense plasma, i.e., $X >>$

https://doi.org/10.5194/angeo-2023-6
Preprint. Discussion started: 28 February 2023

Annales Geophysicae Discussions

Y^2. In plasma wave propagation, the electron plasma density is a determinant parameter in calculating wave group velocity. Outside the plasmasphere, while magnetospheric convection increases, the plasma density can vary from very low density ($\sim 1\ \mathrm{cm}^{-3}$) to increased density values ($\sim 50\ \mathrm{cm}^{-3}$). Though, obtaining wave group velocity from the Appleton-Hartree solution in this environment can be challenging (Anderson et al., 1992).

Recent space missions have provided density measurement with a confidence level of 10% under quiet geomagnetic conditions (Zhelavskaya et al., 2016). Although a more precise measurement is still challenging, we use plasma density data from the EMFISIS instrument (Kletzing et al., 2013) onboard the Van Allen Probes Mission to calculate the wave-particle time of interaction.

The change in the relativistic electron flux can occur in several energy levels because the harmonic resonant number n on the left-hand side Equation 3 allows several electrons' energy to satisfy this condition (see Allison et al., 2021, and references therein). Accordingly, we take the in situ measurements from four examples previously described in the literature by Tu et al. (2014); Liu et al. (2020); Guo et al. (2021) to calculate the pitch angle variation (Eq. 20) due to the parallel propagating chorus wave interacting with electrons from different energies, for a period τ of one wave cycle, as described in the following.

In Figure 5 (and also in Figures A1 and B1), we show in panels (from top to bottom) the whistler-mode chorus waves spectrum, the interpolated 1.8 MeV electron flux pitch angle distribution, the relativistic and low energy electron stacked fluxes, the magnitude of the ambient magnetic field, and the local plasma density. The same format is used in Figures A1 and B1. The case study parameters were measured by the following instruments onboard the Van Allen Probes. The Electric and Magnetic Field Instrument Suite and Integrated Science (EMFISIS) (Kletzing et al., 2013) provides the chorus spectrum measurements. The pitch angle distribution of relativistic electrons is provided by the Relativistic Electron Proton Telescope (REPT) (Baker et al., 2013) and the low-energy electron flux is measured by Magnetic Electron Ion Spectrometer (MAGEISS) (Blake et al., 2013). The Electric Field and Waves Instruments (EFW) (Wygant et al., 2013) provide the ambient magnetic field magnitude. We use the L4 data level from the EMFISIS instrument to plot in Figure 6 the whistler-mode chorus waves' ellipticity, planarity, wave normal angle, and the polar angle of Poynting vector, respectively, from panels (b)-(e) (the same format is used in Figures D1 and E1). The wave parameters were calculated according to Santolik et al. (2003) and the ambient electron density by Zhelavskaya et al. (2016). The whistler mode chorus wave events were selected regarding their ellipticity ($\epsilon \sim 1$), planarity of the magnetic field polarization (≥ 0.8), and wave normal angle (WNA ~ 0). We chose only chorus waves propagating parallel to the ambient magnetic field. To confirm the wave-particle interaction during the case studies, we plot the time evolution of phase space density (PSD [c/(cm MeV))3 sr-1]) as a function of L* calculated through the magnetic field model (TS04) (Tsyganenko and Sitnov , 2005) for μ = 200 MeV/G and 700 MeV/G are presented in Figures 7, F1 and G1. The values of μ correspond to energies 0.37 and 0.92 MeV, respectively, at L* = 5. The data is obtained from the MagEIS instrument onboard Van Allen Probe B, available at https://rbspgway.jhuapl.edu/psd.

Cases 1 and 2 were observed on 08 and 09 October 2012, respectively, and described by Tu et al. (2014). Data provided by the EMFISIS instrument for case 1 (2) are shown in Figure A1 and Figure D1 (B1 and E1). The whistler-mode chorus waves were intensified for almost 7 hours in cases 1 (and 2) from 09-13 (02-09) UT, as shown in panel a A1 (B1), which coincides with the most disturbing periods during this storm. During this interval, the magnetic wave amplitude reached up to 100 pT in

https://doi.org/10.5194/angeo-2023-6
Preprint. Discussion started: 28 February 2023


Annales Geophysicae Discussions

case 1 (Tu et al., 2014). We selected the in situ parameters from the shaded area in Figures A1 and D1 (and from (B1 and E1) for case 2). The one wave cycle period (τ) is available for each case study from high-resolution burst mode magnetic field data from the EMFISIS instruments (e.g., Figure C1). The chorus subelement was chosen in the instant concomitant with the dip in case 1 for the 57-221 keV electron flux energy level. For case 2, the chosen instant coincides with the drop in 1.8 MeV, as shown in Figure B1 panel c. The change in the electron fluxes is observed in several energy levels throughout two consecutive orbits. At satellite apogee, where the measurements are taken, the plasma density was lower than $10\ \mathrm{cm}^{-3}$ for both events.

The phase space density analyses for these cases are shown in Figure F1 and G1. For case 1, Figure F1 presented a locally growing electron PSD peak maximum close to L* = 4.1 and fixed μ = 200 MeV/G, followed by a strong local loss at L* = 4.9 (magenta curve in panel left). The same behavior in minor proportion is observed at fixed μ = 700 MeV/G from 07:35 UT (magenta curve in the panel right). Local loss of electrons is observed from 12:06 UT close to L* = 4.2, more significant at fixed μ = 200 MeV/G (black curve in panel left) compared to fixed μ = 700 MeV/G (black curve in the panel right). This local loss of electrons is followed by the locally growing electron PSD peak close to L* = 4.9 in both fixed μ = 200 MeV/G and μ = 700 MeV/G (see black curves in panels left and right).

For case 2, Figure G1 shows two significant locally growing electron PSD peaks at L* = 4.3 and fixed μ = 200 MeV/G and μ = 700 MeV/G, which are above 370 keV (see green and magenta curves in panels a and b). A local electron flux decrease between L* = 3.9 and 4.3 is observed near 06:09 UT on 2012/10/09 for energies close to 0.6 MeV (see the black curve in panel a), while for energies from above 0.6 MeV, it is observed slight electron flux increase (black curve the panel b). For case 2,

Cases 3 and 4 were observed on 22 December 2014, shown in Figure 5. These events were described by Liu et al. (2020); Guo et al. (2021), and the authors identified them as A and C (we reproduce this identification in Figures 6). The period selected at A shows a minor decrease at the outer radiation belt electron flux around 80 keV as chorus waves are detected among the $0.1\Omega_{ce} < \omega < 0.45\Omega_{ce}$. Differently, at period C, it is shown loss of relativistic electron concomitant with the whistler-mode chorus waves emission at extremely low frequency, i.e., $\omega < 0.1\Omega_{ce}$. In Figure 6, we show the main chorus wave parameters for these events (Liu et al., 2020). According to panel (a), these events correspond to a period of enhanced chorus wave activity. The occurrence of chorus waves is confirmed by the parameters on panels (b) and (c). The WNA in panel (d) remained close to zero, indicating Chorus wave propagates parallel or anti-parallel to the ambient magnetic field line. Also, the polar angle of the Poynting vector in panel (e) shows an alternation between anti-parallel propagation ($180°$) in the shaded region A and quasi-parallel ($0°$) propagation in region C. According to Teng et al. (2018), the change in the polar angle of the Poything vector can be related to a region of chorus wave generation. In such a region, the wave propagation direction can be elsewhere.

Additionally, the phase space density analysis is shown in Figure 7, which shows the local electron flux decrease close to L* = 5 (μ = 200 MeV/G) and L* = 4.5 (μ = 700 MeV/G) near 21:42 UT on 2014/12/21 (blue curves in panels a and b). An expressive electron flux decrease (more than three orders of magnitude) is observed again near 02:12 UT on 2014/12/22 for energies from 0.37 MeV (green curves in panels a and b). This second electron flux decrease is also discussed in Figure 5. From period A to C in Figure 5, the satellite traveled toward the perigee, so the plasma density and the ambient magnetic field strength were enhanced; however, the satellite was outside the plasmasphere all the way it traveled in these intervals. The loss of electrons is observed at least in two energy levels, at 80 keV and later at 2.6 MeV.

https://doi.org/10.5194/angeo-2023-6
Preprint. Discussion started: 28 February 2023


Annales Geophysicae Discussions

Table 1 summarizes the input parameters (from the case studies) used in Equations 5, 13, 20. Besides, the results for the electron's resonant kinetic energy (K_{res}), time of interaction calculated using the special relativity theory approach (T_r) and with a non-relativistic approach (T_{nr}), $\Delta\alpha_r$ that is the resulting pitch angle scattering considering for T_r, and $\Delta\alpha_{nr}$ calculated for T_{nr}.

The ambient magnetic field magnitude B_0, electron plasma density n_e, wave frequency (f_w), wave magnetic field maximum amplitude (B_w), and one wave cycle period (τ) are the input parameters. The electron resonant kinetic energy results (K_{res}) according to Eq. 5 for one or two gyrofrequency harmonics (informed in parentheses). For comparison purposes, we show the change in pitch angle considering the relativistic interaction time ($\Delta\alpha_r$) and also considering the non-relativistic interaction time ($\Delta\alpha_{nr}$), both calculated from Eq. 20. In all four cases, we verified from EMFISIS data that chorus waves propagate parallel to the ambient magnetic field (WNA $\theta = 0$), and the equatorial initial pitch angle for the relativistic electron (from REPT) was 90^0. The same equatorial pitch angle was assumed for low-energy particles.

The interaction time shows a significant dependence on the wave group velocity and the relativistic addition velocity, initial pitch angle, and gyrofrequency harmonic. Thus, according to Table 1, the time of interaction observed in the S frame (i.e., in the satellite frame) can be 2-times longer than the time of interaction in the electron's frame (S'), i.e., without relativistic calculation, leading to a similar difference to the change in pitch angle as it is proportional to the time of interaction.

5 Conclusion

In this article, we consider the kinematics of Special Relativity to derive a consistent formula to the time of interaction equation applied to wave-particle interaction between whistler mode chorus waves and high-energy electrons. In the derivation, we considered that the wave-particle interaction occurs in the electron's reference frame, and the electron flux pitch angle is measured in the satellite reference frame. We consider the scale factor length contraction and the time dilatation effects to relate the parameters from one reference frame to the other, as well as the relativistic transformation of velocities. Thus we use in situ plasma parameters provided by Van Allen Probes (in Eq. 2 and 4) during quiet geomagnetic conditions to estimate the general variation of the time of interaction regarding the electron resonant kinetic energy.

We found that the inappropriate calculation of the time of interaction, ignoring or misleading the special relativity theory context, under-estimate the time of interaction at around 30%, even for the lowest resonant electron kinetic energy. Consequently, the pitch angle change is also underestimated if the relativistic approach is misunderstood. The magnetospheric parameters can change significantly at different solar wind drivers. Actually, under disturbed conditions, the underestimation (in time and change in pitch angle) can be even higher, as shown in Table 1. Furthermore, our results show that the longest time of interaction occurs at wave-particle interaction with high pitch angle electrons, with energy $\sim 100's$ of keV, interacting with quasi-parallel propagating waves. This energy dependence happens due to the peak in the wave group velocity (v_g) resonant to the low energy electrons. Accordingly, v_g decreases as the wave frequency approach the Ω_{ce} and become resonant to the higher energy electrons.

https://doi.org/10.5194/angeo-2023-6
Preprint. Discussion started: 28 February 2023


Annales Geophysicae Discussions

Whistler-mode chorus waves group velocity at the magnetosphere is a fraction of the speed of light. The propagating waves can interact with high-energy electrons bouncing in the magnetic field lines. Regarding the velocities magnitude involved in this interaction, this problem relays on the Special Relativity domain. Thus, the special relativity approach has to be considered in calculating the resonant Doppler shift condition, in the interaction time, and in the change of the pitch angle.

The group velocity and the correspondent resonant electron kinetic energy equations are derived here for parallel or oblique whistler-mode chorus waves. They can be applied to any whistler dispersion relation in cold plasma.

Finally, the correct calculation of the interaction time, i.e., made with complete Special Relativity considerations, benefits modeling of the Earth's outer radiation belt electron flux since they improve the estimates and the prediction of pitch angle change due to wave-particle interaction.

Data availability. All the data used are available:

ECT: https://cdaweb.gsfc.nasa.gov/pub/data/rbsp/
EFW: http://themis.ssl.berkeley.edu/data/rbsp/efwcmds/
EMFISIS: https://emfisis.physics.uiowa.edu/Flight/

Appendix A: Case studies

In this section, we show the Van Allen Probes data measurements for cases 1 and 2 related to the whistler-mode chorus waves magnetic field spectrum, the interpolated 1.8 MeV electron flux pitch angle distribution, the relativistic and low energy electron fluxes, the ambient magnetic field, and the local plasma density. Also, it is shown the whistler mode chorus waves ellipticity, planarity, WNA – wave Normal angle, and the polar angle of the Poynting vector. The parameters are taken from the period highlighted in the gray-shaded area. They are used to calculate the time of interaction and change in pitch angle for the energy of the resonant electrons shown in Table 1.

Also, for cases 1 and 2, we selected some periods of interest to confirm wave-particle interaction takes place during these events. We show in this section the measurements of the time evolution of phase space density (PSD) radial profiles at fixed first adiabatic invariant, μ=200MeV/G and μ=700MeV/G and second (K=0.11G1/2RE) adiabatic invariant for both inbound and outbound parts of the RBSP-B orbit.

Author contributions. L.R. Alves wrote the paper, evaluated the equations related to the cold plasma waves and resonant kinetic energy, revised the special relativity kinematic equations, and also performed the case studies data analyses based on the Van Allen Probes dataset. M.E.S. Alves wrote the paper, evaluated the special relativity kinematic equations, and revised the cold plasma waves equations. L.A. da Silva revised the paper and performed the Phase Space Density analyses for the outer radiation belt electrons. V. Deggeronni revised the paper, wrote the codes for plotting the whistler mode chorus waves parameters, and contributed to the case studies data analyses based on the

https://doi.org/10.5194/angeo-2023-6
Preprint. Discussion started: 28 February 2023

Van Allen Probes dataset. P. Jauer revised the paper and contributed to the discussions of case studies based on the Van Allen Probes dataset.
330 D. G. Sibeck is the Project Scientist of the Van Allen Probes Mission contributing to the manuscript case studies discussions

Competing interests. The authors declare no competing interests are present in the manuscript.

Acknowledgements. We thank the Brazilian Ministry of Science, Technology, and Innovation and the Brazilian Space Agency. L. R. Alves, thanks for the financial support by CNPq through PQ-grant number 309026/2021-0. L.A.S. and P.J. are grateful for financial support from the China-Brazil Joint Laboratory for Space Weather (CBJLSW), National Space Science Center (NSSC), and the Chinese Academy
335 of Science (CAS). This research was also supported by the International Partnership Program of Chinese Academy of Sciences (grants 183311KYSB20200003 and 183311KYSB20200017). L.R. Alves thanks to the Autoplot platform. We acknowledge the NASA Van Allen Probes, Harlan E. Spence [PI ECT; University of New Hampshire], Craig Kletzing [PI EMFISIS; University of Iowa], and John R. Wygant [PI EFW; University Minnesota] for the use of data.

https://doi.org/10.5194/angeo-2023-6
Preprint. Discussion started: 28 February 2023

Annales Geophysicae Discussions

References

Allison H J, Shprits Y. Y., Zhelavskaya I. S., Wang D. and Smirnov A. G., Gyroresonant wave-particle interactions with chorus waves during extreme depletions of plasma density in the Van Allen radiation belts, Science Advances, 7, doi:10.1126/sciadv.abc0380, 2021.

Alves, L. R., et al., Outer radiation belt dropout dynamics following the arrival of two interplanetary coronal mass ejections, Geophys. Res. Lett., 43, 978– 987, doi:10.1002/2015GL067066, 2016.

Anderson, R. R., D. A. Gurnett, and D. L. Odem, CRRES plasma wave experiment, J. Spacecr. Rockets, 29(4), 570–573, doi: 10.2514/3.25501, 1992.

A. Artemyev, O. Agapitov, D. Mourenas, D. et al. Oblique Whistler-Mode Waves in the Earth's Inner Magnetosphere: Energy Distribution, Origins, and Role in Radiation Belt Dynamics. Space Sci Rev 200, 261–355, https://doi.org/10.1007/s11214-016-0252-5, 2016.

Baker, D., et al., The relativistic electron-proton telescope (rept) instrument on board the radiation belt storm probes (rbsp) spacecraft: Characterization of earth's radiation belt high-energy particle populations, in The Van Allen Probes Mission, edited by N. Fox and J. L. Burch, pp. 337–381, Springer, New York,doi:$10.1007/978-1-4899-7433-4_11$, 2013.

Blake, J.B. et al., The Magnetic Electron Ion Spectrometer (MagEIS) Instruments Aboard the Radiation Belt Storm Probes (RBSP) Spacecraft. In: Fox, N., Burch, J.L. (eds) The Van Allen Probes Mission. Springer, Boston, MA. https://doi.org/10.1007/978-1-4899-7433-4–12, 2013.

Bittencourt, J.A., Fundamentals of Plasma Physics. Edition 3. Springer, New York, NY. https://doi.org/10.1007/978-1-4757-4030-1, 1995.

Bortnik, J., Inan, U. S., and Bell, T. F., Landau damping and resultant unidirectional propagation of chorus waves, Geophys. Res. Lett., 33, L03102, doi:10.1029/2005GL024553, 2006.

Bortnik, J., Thorne, R. M., and Inan, U. S., Nonlinear interaction of energetic electrons with large amplitude chorus, Geophys. Res. Lett., 35, L21102, doi:10.1029/2008GL035500, 2008.

L. A. Da Silva, J. Shi, L. R. Alves, D. Sibeck, J. P. Marchezi, C. Medeiros, L. E. A. Vieira, O. Agapitov, F. R. Cardoso, V. M. Souza, A. Dal Lago, P. R. Jauer, C. Wang, H. Li, Z. Liu, M. V. Alves, M. S. Rockenbach, High-Energy Electron Flux Enhancement Pattern in the Outer Radiation Belt in Response to the Alfvénic Fluctuations Within High-Speed Solar Wind Stream: A Statistical Analysis, Journal of Geophysical Research: Space Physics, 126, 8, 10.1029/2021JA029363, 2021.

Guo, D., Xiang, Z., Ni, B., Cao, X., Fu, S., Zhou, R., et al., Bounce resonance scattering of radiation belt energetic electrons by extremely low-frequency chorus waves. Geophysical Research Letters, 48, e2021GL095714. https://doi.org/10.1029/2021GL095714, 2021.

Helliwell, R.A., Whistlers and Related Ionospheric Phenomena. Edition 3. Stanford University Press, Stanford, 1965.

Horne, R. B., and Thorne, R. M., Relativistic electron acceleration and precipitation during resonant interactions with whistler-mode chorus, Geophys. Res. Lett., 30, 1527, doi:10.1029/2003GL016973, 10, 2003a.

Horne, R. B., Glauert, S. A., and Thorne, R. M., Resonant diffusion of radiation belt electrons by whistler-mode chorus, Geophys. Res. Lett., 30, 1493, 9, doi:10.1029/2003GL016963, 2003b.

Hsieh, Y.-K., Kubota, Y., Omura, Y., Nonlinear evolution of radiation belt electron fluxes interacting with oblique whistler mode chorus emissions. Journal of Geophysical Research: Space Physics, 125, e2019JA027465. https://doi.org/10.1029/2019JA027465, 2020.

Hsieh, Y.-K., Omura, Y., Kubota, Y., Energetic electron precipitation induced by oblique whistler mode chorus emissions. Journal of Geophysical Research: Space Physics, 127, e2021JA029583. https://doi.org/10.1029/2021JA029583, 2022.

Hua, M., Bortnik, J., and Ma, Q., Upper limit of outer radiation belt electron acceleration driven by whistler-mode chorus waves. Geophysical Research Letters, 49, e2022GL099618. https://doi.org/10.1029/2022GL099618, 2022.

https://doi.org/10.5194/angeo-2023-6
Preprint. Discussion started: 28 February 2023

Jaynes, A. N., Baker D. N., Singer, H. J., Rodriguez, J. V., Loto'aniu, T. M., Ali, A. F., Elkington, S. R., Li, X., Kanekal, S. G., Claudepierre, S. G., Fennell, J. F., Li, W., Thorne, R. M., Kletzing C. A., Spence H. E., Reeves, G. D., Source and seed populations for relativistic electrons: Their roles in radiation belt changes, J. Geophys. Res. Space Physics, 120, 7240– 7254, doi:10.1002/2015JA021234, 2015

Kletzing, C.A., Kurth, W.S., Acuna, M. et al. The Electric and Magnetic Field Instrument Suite and Integrated Science (EMFISIS) on RBSP. Space Sci Rev 179, 127–181. https://doi.org/10.1007/s11214-013-9993-6, 2013

Lam, Mai Mai and Horne, Richard B. and Meredith, Nigel P. and Glauert, Sarah A. and Moffat-Griffin, Tracy and Green, Janet C. Origin of energetic electron precipitation >30 keV into the atmosphere. Journal of Geophysical Research: Space Physics, 115, A4, https://agupubs.onlinelibrary.wiley.com/doi/pdf/10.1029/2009JA014619, 2010

G. S. Lakhina, B. T. Tsurutani, O. P. Verkhoglyadova, and J. S. Pickett, Pitch angle transport of electrons due to cyclotron interactions with the coherent chorus subelements, J. Geophys. Res., 115, A00F15, doi:10.1029/2009JA014885, 2010

Solène Lejosne, Hayley J. Allison, Lauren W. Blum, Alexander Y. Drozdov, Michael D. Hartinger, Mary K. Hudson, Allison N. Jaynes, Louis Ozeke, Elias Roussos, Hong Zhao, Differentiating Between the Leading Processes for Electron Radiation Belt Acceleration, Frontiers in Astronomy and Space Sciences, 9, doi: 10.3389/fspas.2022.896245. 2022.

Li, J.,Ni, B., Xie, L., Pu, Z., Bortnik, J., Thorne, R. M., Chen, L., Ma, Q., Fu, S., Zong, Q., Wang, X., Xiao, C., Yao, Z., Guo, R., Interactions between magnetosonic waves and radiation belt electrons: Comparisons of quasi-linear calculations with test particle simulations, Geophys. Res. Lett., 41, 4828– 4834, doi:10.1002/2014GL060461, 2014.

Liu, S., Xie, Y., Zhang, S., Shang, X., Yang, C., Zhou, Q., He, Y., Xiao, F., Unusual loss of Van Allen belt relativistic electrons by extremely low-frequency chorus. Geophysical Research Letters, 47, e2020GL089994. https://doi.org/10.1029/2020GL089994, 2020.

Lorentzen, K. R., Blake, J. B., Inan, U. S., Bortnik, J., Observations of relativistic electron microbursts in association with VLF chorus, J. Geophys. Res., 106(A4), 6017– 6027, doi:10.1029/2000JA003018, 2001.

Mourenas, D., Artemyev, A. V., Agapitov, O. V., Krasnoselskikh, V., and Mozer, F. S., Very oblique whistler generation by low-energy electron streams. J. Geophys. Res. Space Physics, 120, 3665– 3683. doi: 10.1002/2015JA021135, 2015.

Orlova, K. G., Shprits, Y. Y., and Ni, B., Bounce-averaged diffusion coefficients due to resonant interaction of the outer radiation belt electrons with oblique chorus waves computed in a realistic magnetic field model, J. Geophys. Res., 117, A07209, doi:10.1029/2012JA017591, 2012.

Omura, Y. Nonlinear wave growth theory of whistler-mode chorus and hiss emissions in the magnetosphere. Earth Planets Space 73, 95, https://doi.org/10.1186/s40623-021-01380-w, 2021.

Reeves, G. D., McAdams, K. L., Friedel, R. H. W., and O'Brien, T. P., Acceleration and loss of relativistic electrons during geomagnetic storms, Geophys. Res. Lett., 30, 1529, 10, doi:10.1029/2002GL016513, 2003

Reeves, G. D., Spence, H. E., Henderson, M. G., Morley, S. K., Fiedel, R. H. W., Funsten, H. O., Baker, D. N., Kanekal S. G., Blake, J. B., Fennell, J. F., Claudepierre, S. G., Thorne, R. M., Turner, D. L., Kletzing, C. A., Kurth, W. S., Larsen, B. A., Niehof, J. T., Electron Acceleration in the Heart of the Van Allen Radiation Belts, Science, 341, 6149, doi:10.1126/science.1237743, 2013

Santolík, O., Parrot, M., and Lefeuvre, F., Singular value decomposition methods for wave propagation analysis, Radio Sci., 38, 1010, 1, doi:10.1029/2000RS002523, 2003.

Santolík, O., Gurnett, D. A., Pickett, J. S., Chum, J., and Cornilleau-Wehrlin, N., Oblique propagation of whistler mode waves in the chorus source region, J. Geophys. Res., 114, A00F03, doi:10.1029/2009JA014586, 2009.

https://doi.org/10.5194/angeo-2023-6
Preprint. Discussion started: 28 February 2023

Sicard-Piet, A., Boscher, D., Horne, R. B., Meredith, N. P., and Maget, V.: Effect of plasma density on diffusion rates due to wave particle interactions with chorus and plasmaspheric hiss: extreme event analysis, Ann. Geophys., 32, 1059–1071, https://doi.org/10.5194/angeo-32-1059-2014, 2014.

Shprits, Y. Y., Meredith, N. P., and Thorne, R. M., Parameterization of radiation belt electron loss timescales due to interactions with chorus waves, Geophys. Res. Lett., 34, L11110, doi:10.1029/2006GL029050, 2007.

Shprits, Y. Y., Elkington, S. R., Meredith, N. P., and Subbotin, D. A., Review of modeling of losses and sources of relativistic electrons in the outer radiation belt I: Radial transport. Journal of Atmospheric and Solar-Terrestrial Physics, 70(14), 1679–1693. doi:10.1016/j.jastp.2008.06.00, 2008

Subbotin, D., Shprits, Y., and Ni, B., Three-dimensional VERB radiation belt simulations including mixed diffusion, J. Geophys. Res., 115, A03205, doi:10.1029/2009JA015070, 2010.

Summers, D., Ni, B., and Meredith, N. P., Timescales for radiation belt electron acceleration and loss due to resonant wave-particle interactions: 1. Theory, J. Geophys. Res., 112, A04206, doi:10.1029/2006JA011801, 2007.

Summers, D., Y. Omura, Y. Miyashita, and D.-H. Lee, Nonlinear spatiotemporal evolution of whistler modechorus waves in Earth's inner magnetosphere,J. Geophys. Res.,117, A09206, doi:10.1029/2012JA017842, 2012.

Teng, S., Tao, X., Li, W., Qi, Y., Gao, X., Dai, L., Lu, Q., e Wang, S. A statistical study of the spatial distribution and source-region size of chorus waves using Van Allen Probes data. Ann. Geophys., 36, 867–878, https://doi.org/10.5194/angelo-36-867-2018, 2018.

Thorne, R.M., Horne, R.B., Glauert, S., Meredith, N.P., Shprits, Y.Y., Summers, D. and Anderson, R.R., The Influence of Wave-Particle Interactions on Relativistic Electron Dynamics During Storms. In Inner Magnetosphere Interactions: New Perspectives from Imaging (eds J. Burch, M. Schulz and H. Spence). https://doi.org/10.1029/159GM07, 2005.

Tsurutani, Bruce T. and Lakhina, Gurbax S. and Verkhoglyadova, Olga P. Energetic electron (>10 keV) microburst precipitation, 5–15 s X-ray pulsations, chorus, and wave-particle interactions: A review. Journal of Geophysical Research: Space Physics, 118,5, 2296-2312, https://doi.org/10.1002/jgra.50264, 2013.

Tsurutani, B. T., and Lakhina, G. S., Some basic concepts of wave-particle interactions in collisionless plasmas, Rev. Geophys., 35(4), 491–501, doi:10.1029/97RG02200, 1997.

Tsurutani, B. T., and Smith, E. J., Postmidnight chorus: A substorm phenomenon, J. Geophys. Res., 79(1), 118– 127, doi:10.1029/JA079i001p00118, 1974.

Tsurutani, B. T. and Smith, E. J. Two types of magnetospheric ELF chorus and their substorm dependences. Journal of Geophysical Research (1896-1977), 82, 32, 5112-5128, https://doi.org/10.1029/JA082i032p05112, 1977.

Tsyganenko, N. A., Sitnov, M. I. Modeling the dynamics of the inner magnetosphere during strong geomagnetic storms. Journal of Geophysical Research, 110, A03208. https://doi.org/10.1029/2004JA010798, 2005

Tu, W., Cunningham, G. S., Chen, Y., Morley, S. K., Reeves, G. D., Blake, J. B., Baker, D. N., and Spence, H., Event-specific chorus wave and electron seed population models in DREAM3D using the Van Allen Probes, Geophys. Res. Lett., 41, 1359– 1366, doi:10.1002/2013GL058819, 2014.

Verkhoglyadova, O. P., Tsurutani, B. T., and Lakhina, G. S., Properties of obliquely propagating chorus, J. Geophys. Res., 115, A00F19, doi:10.1029/2009JA014809, 2010.

Zhang, X.-J., Mourenas, D., Artemyev, A. V., Angelopoulos, V., and Thorne, R. M., Contemporaneous EMIC and whistler mode waves: Observations and consequences for MeV electron loss, Geophys. Res. Lett., 44, 8113– 8121, doi:10.1002/2017GL073886, 2017.

https://doi.org/10.5194/angeo-2023-6
Preprint. Discussion started: 28 February 2023

Zhelavskaya, I. S., Spasojevic, M., Shprits, Y. Y., and Kurth, W. S., Automated determination of electron density from electric field measurements on the Van Allen Probes spacecraft, J. Geophys. Res. Space Physics, 121, 4611– 4625, doi:10.1002/2015JA022132, 2016.

Walker, A.D.M., The Effect of Wave Fields on Energetic Particles. In: Plasma Waves in the Magnetosphere. Physics and Chemistry in Space Planetology, vol 24. Springer, Berlin, Heidelberg. https://doi.org/10.1007/978-3-642-77867-4–8, 1993.

Wygant, J.R., and Bonnell, J. W. Goetz, K., Ergun, R. E., Mozer, F. S., Bale, S. D., Ludlam, M., Turin, P., Harvey, P. R., Hochmann, R., Harps, K., Dalton, G., McCauley, J., Rachelson, W., Gordon, D., Donakowski, B., Shultz, C., Smith, C., Diaz-Aguado, M., Fischer, J., Heavner, S., Berg, P., Malsapina, D. M., Bolton, M. K., Hudson, M., Strangeway, R. J., Baker, D. N., Li, X., Albert, J., Foster, J. C., Chaston, C. C., Mann, I., Donovan, E., Cully, C. M., Cattell, C. A., Krasnoselskikh, V., Kersten, K., Brenneman, A., Tao, J. B. The Electric Field and Waves Instruments on the Radiation Belt Storm Probes Mission. In: Fox, N., Burch, J.L. (eds) The Van Allen Probes Mission. Springer, Boston, MA. https://doi.org/10.1007/978-1-4899-7433-4–6, 2013

https://doi.org/10.5194/angeo-2023-6
Preprint. Discussion started: 28 February 2023

Annales Geophysicae Discussions
Open Access
EGU

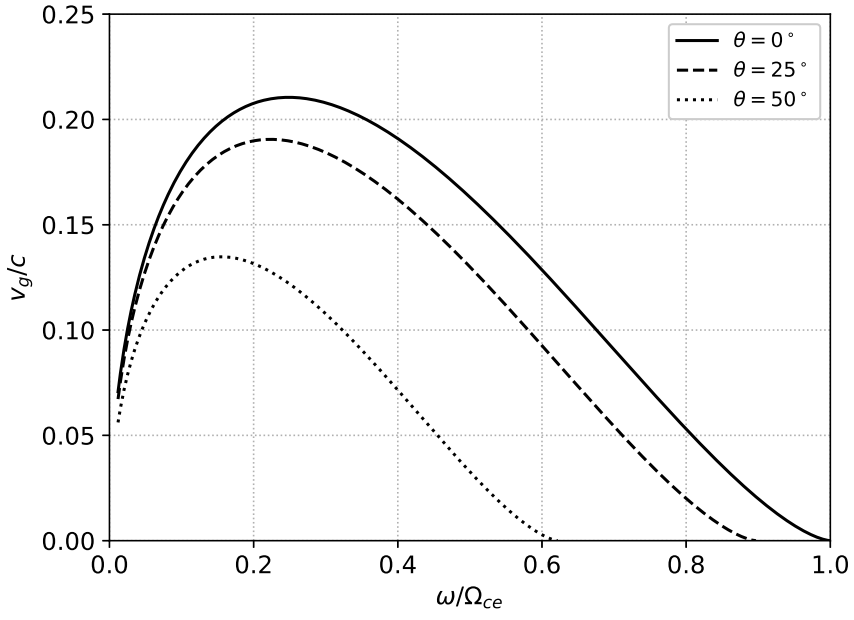

Figure 1. Group velocity v_g/c as a function of whistler-mode chorus waves frequency to the plasma gyrofrequency for three different wave normal angles propagation. This group velocity is the full solution of Appleton-Hartree for whistler waves propagating in low-density plasma media at any orientation. Plasma parameters used in the calculation are provided by the Van Allen Probes apogee orbit, $B_0 = 150$ nT, and low density $n = 2\ \mathrm{cm}^{-3}$.

https://doi.org/10.5194/angeo-2023-6
Preprint. Discussion started: 28 February 2023

Annales Geophysicae Discussions
Open Access
EGU

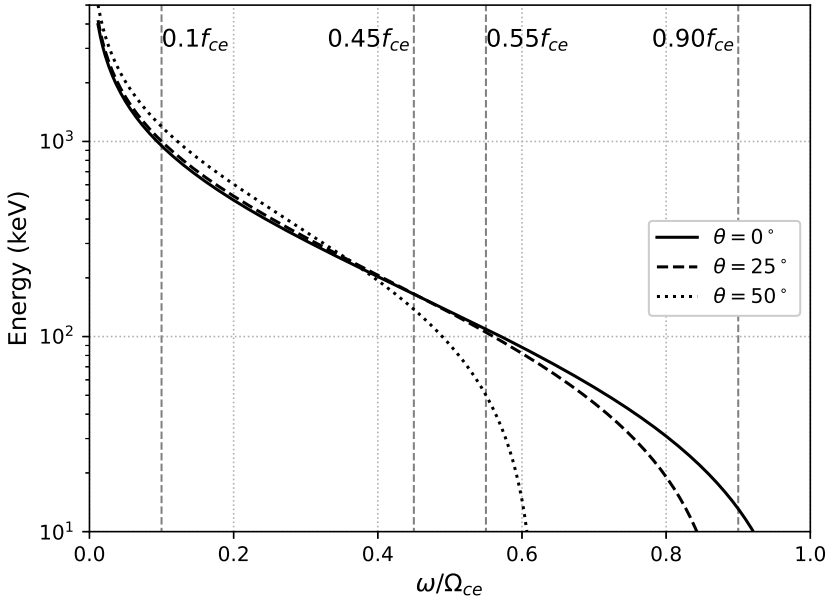

Figure 2. Electron resonant kinetic energy (KeV) as a function of whistler mode chorus wave frequency normalized by the electron gyrofrequency propagating at different WNA (θ) 0 (parallel), 25^o (quasi-parallel) and 50^o (oblique) (b) to the ambient magnetic field ($B_0 = 120nT$). The wave-particle resonance condition depends on the wave dispersion relation ($\omega/\boldsymbol{k}$), calculated from Eq.2, with n = 3. The vertical lines delimitate the low-band whistler mode chorus wave frequency correspondent to $0.1f_{ce} \leq f \leq 0.45f_{ce}$ and the high-band $0.55f_{ce} \leq f \leq 0.90f_{ce}$ as a fraction of the electron gyrofrequency. Plasma parameters are the same as used in Figure 1

https://doi.org/10.5194/angeo-2023-6
Preprint. Discussion started: 28 February 2023

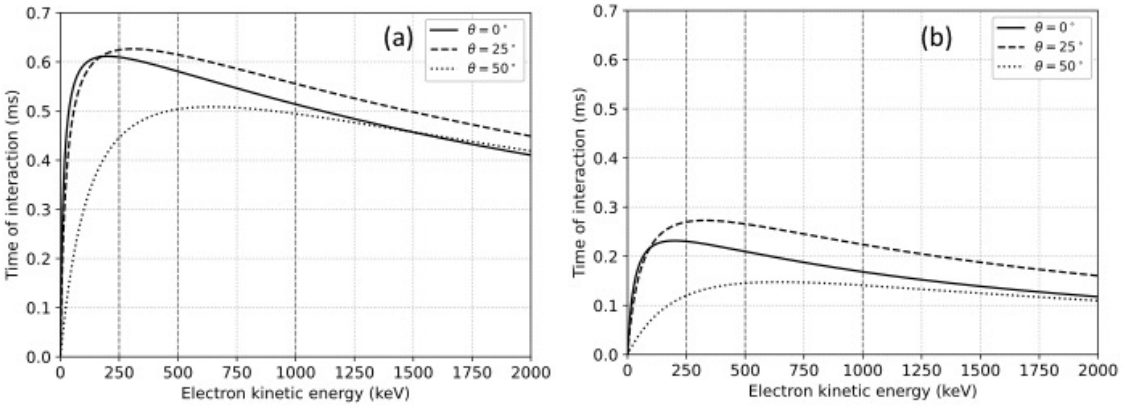

Figure 3. Time of interaction (ms) for (a) $\alpha = 80°$, and (b) $\alpha = 25°$ as a function of electron resonant kinetic energy (keV) for three different wave normal angles propagation. Vertical lines indicate the time of interaction for the resonant wave-particle interaction with $1500, 840, 400$ Hz, and the correspondent electron energy. Plasma parameters used in the calculation are the same as used in the other Figures

https://doi.org/10.5194/angeo-2023-6
Preprint. Discussion started: 28 February 2023

Annales Geophysicae Discussions
Open Access
EGU

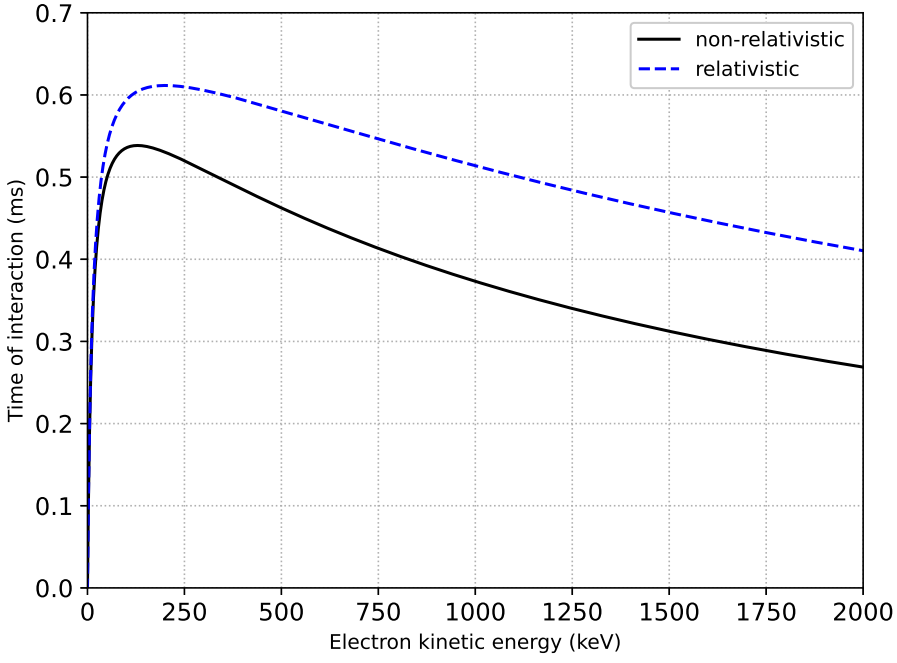

Figure 4. Comparison of time of interaction (ms) as a function of electron resonant kinetic energy (keV) calculated from non-relativistic approach (black line) and full relativistic correction (blue line). Vertical lines indicate the time of interaction for Plasma parameters are the same as in Figure 1

https://doi.org/10.5194/angeo-2023-6
Preprint. Discussion started: 28 February 2023

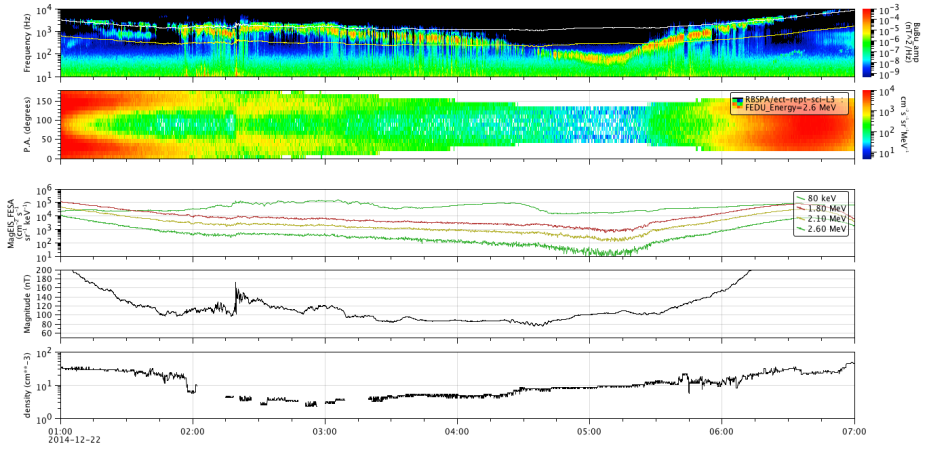

Figure 5. Panels show from top to bottom the whistler-mode chorus waves spectrum, the interpolated 1.8 MeV electron flux pitch angle distribution, the relativistic and low energy electron fluxes, the ambient magnetic field, and the local plasma density. The parameters shown in the A and C regions were used to calculate the time of interaction and change in pitch angle for the resonant electrons energy shown in table 1

https://doi.org/10.5194/angeo-2023-6
Preprint. Discussion started: 28 February 2023

Annales Geophysicae Discussions
Open Access
EGU

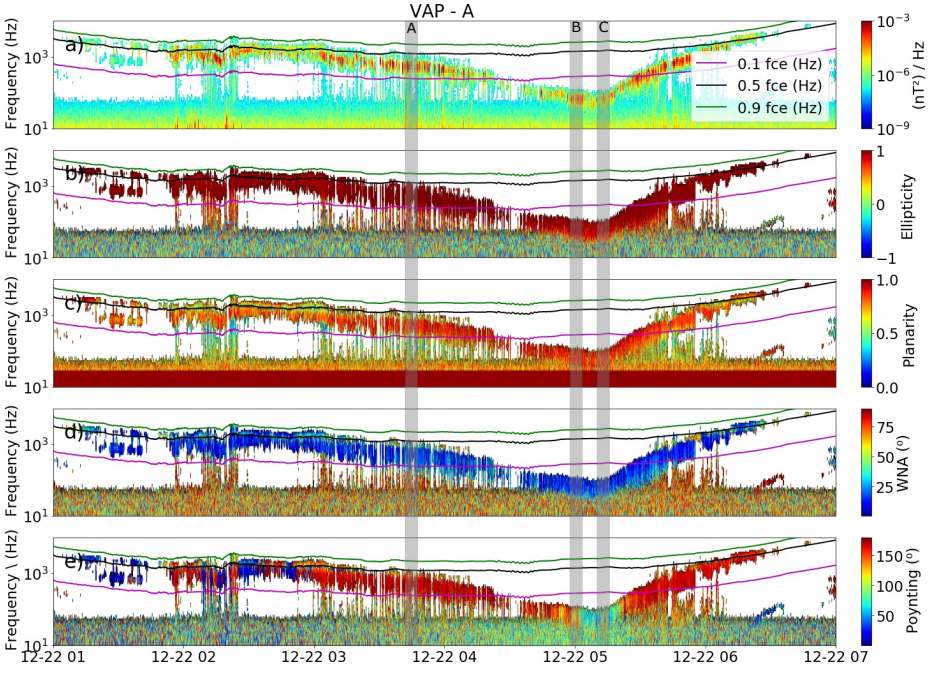

Figure 6. Panels show the whistler-mode chorus waves (a) spectrum of the magnetic field, (b) ellipticity; (c) planarity; (d) WNA – wave Normal angle; (e) the polar angle of Poynting vector. In all panels, the t values of 0.1fce (Hz), 0.5fce (Hz), and 0.9 fce (Hz) are shown by the pink, black, and green lines, respectively. The parameters shown in the A and C regions were used to calculate the time of interaction and change in pitch angle for the resonant electrons energy shown in table 1

https://doi.org/10.5194/angeo-2023-6
Preprint. Discussion started: 28 February 2023

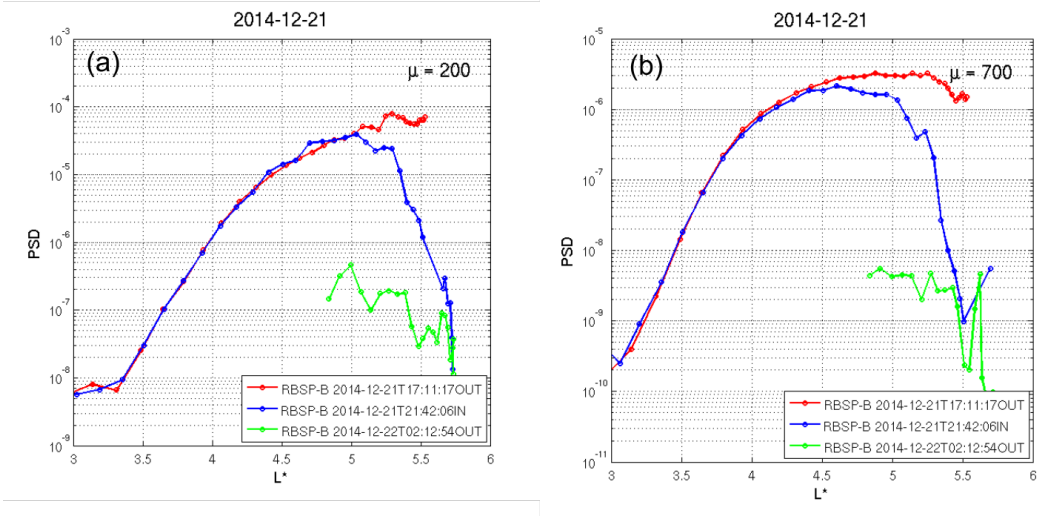

Figure 7. Time evolution of phase space density (PSD [c/(cm MeV))3 sr-1]) radial profiles at fixed first adiabatic invariant, μ=200MeV/G (a) and μ=200MeV/G (b), and second (K=0.11G1/2RE) adiabatic invariant for both inbound and outbound parts of the RBSP-B orbit. Period of analyzes: 21 Dec 2014 at 17:11:17 UT to 22 Dec 2014 at 02:12:54 UT.

https://doi.org/10.5194/angeo-2023-6
Preprint. Discussion started: 28 February 2023

Annales Geophysicae Discussions
Open Access
EGU

Table 1. Input parameters used in the Equations of sections 2, 3, and 4 used to calculate the chorus wave-particle time of interaction and the change in pitch angle for cases 1 to 4. The subscript r and nr means relativistic and non-relativistic, respectively.

Input parameters						Results				
Cases	B_0 [nT]	n_e [cm^{-3}]	f_w [Hz]	B_w [nT]	τ [ms]	K_{res} [keV]	T_r [ms]	T_{nr} [ms]	$\Delta\alpha_r$ [^{o}]	$\Delta\alpha_{nr}$ [^{o}]
1	106	6.2	420	1.64	0.85	180 (3)	0.30	0.34	0.68	0.73
						1200(10)	0.27	0.11	0.24	0.11
2	130	2.6	440	1.64	1.10	300 (2)	0.55	0.49	1.04	0.98
						1780(7)	0.50	0.20	0.32	0.31
3	89	5.0	420	1.37	1.28	130 (3)	0.53	0.49	1.03	0.98
4	106	9.7	79	0.24	5.0	1800 (5)	0.81	0.40	0.10	0.06
						2100(8)	0.81	0.47	0.07	0.07

Cases 1 and 2 (Tu et al., 2014) - from 8 October 2012 (dropout) and 9 October 2022 (repopulation). Cases 3 and 4 (Liu et al., 2020) - 22 December 2014, 00:00 - 06:00 (UTC)

https://doi.org/10.5194/angeo-2023-6
Preprint. Discussion started: 28 February 2023

Annales Geophysicae Discussions
Open Access
EGU

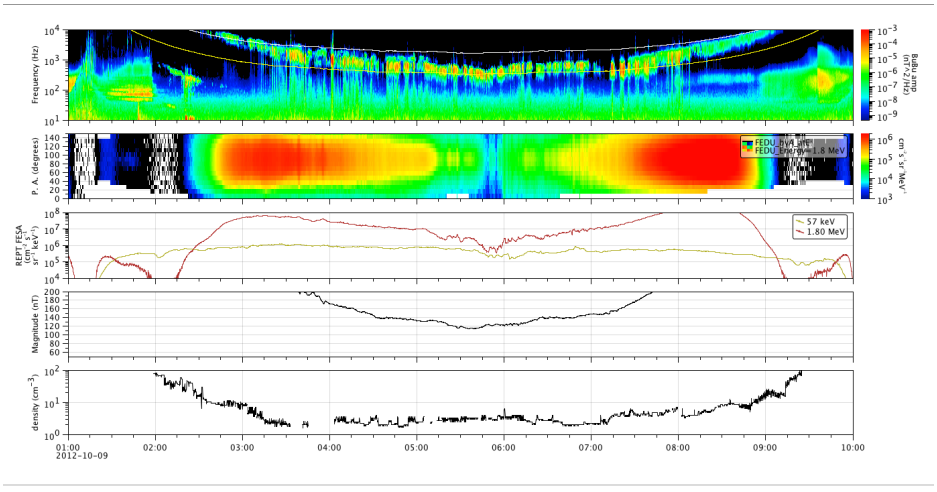

Figure A1. Panels show from top to bottom the whistler-mode chorus waves spectrum, the interpolated 1.8 MeV electron flux pitch angle distribution, the relativistic and low energy electron fluxes, the ambient magnetic field, and the local plasma density for the whistler mode chorus waves observed on 09 October 2012. The parameters shown in the highlighted area were used to calculate the time of interaction and change in pitch angle for the energy of the resonant electrons shown in table 1.

https://doi.org/10.5194/angeo-2023-6
Preprint. Discussion started: 28 February 2023

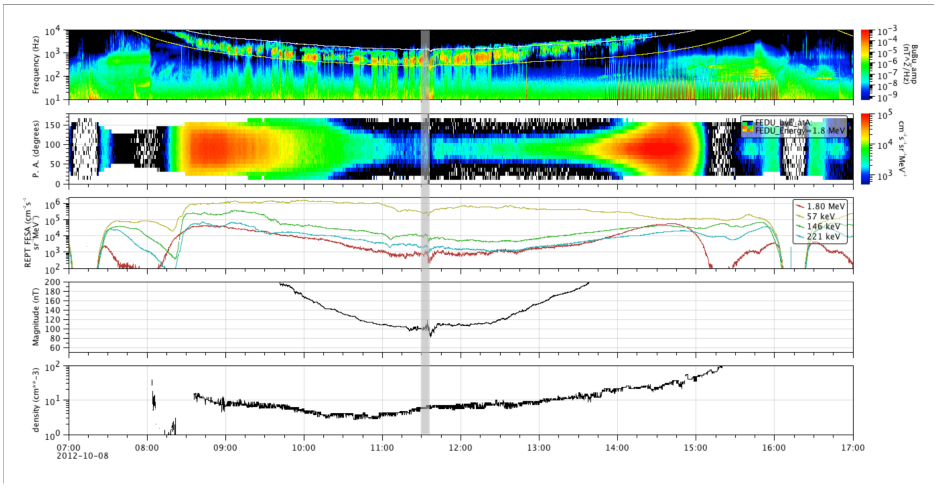

Figure B1. Panels show from top to bottom the whistler-mode chorus waves spectrum, the interpolated 1.8 MeV electron flux pitch angle distribution, the relativistic and low energy electron fluxes, the ambient magnetic field, and the local plasma density observed on 08 October 2012. The parameters shown in the highlighted area were used to calculate the time of interaction and change in pitch angle for the energy of the resonant electrons shown in table 1.

https://doi.org/10.5194/angeo-2023-6
Preprint. Discussion started: 28 February 2023

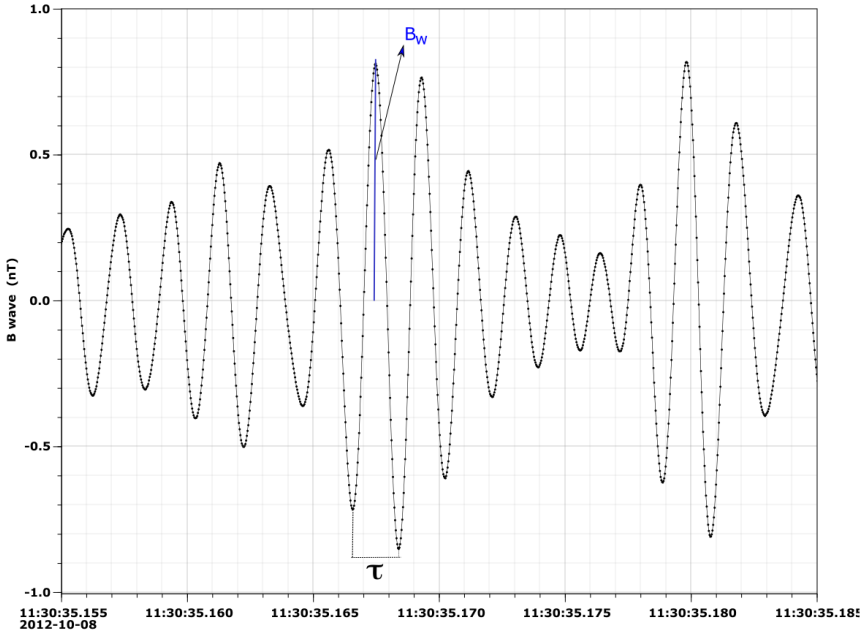

Figure C1. The high-resolution magnetic field measurement related to the event on 08 Oct 2012 during the higher magnetic field spectral density shown in Figure B1. The same plot was made for the other three studied events. The figure identifies the maximum instantaneous wave magnetic field amplitude B_w and the one wave cycle period τ.

https://doi.org/10.5194/angeo-2023-6
Preprint. Discussion started: 28 February 2023

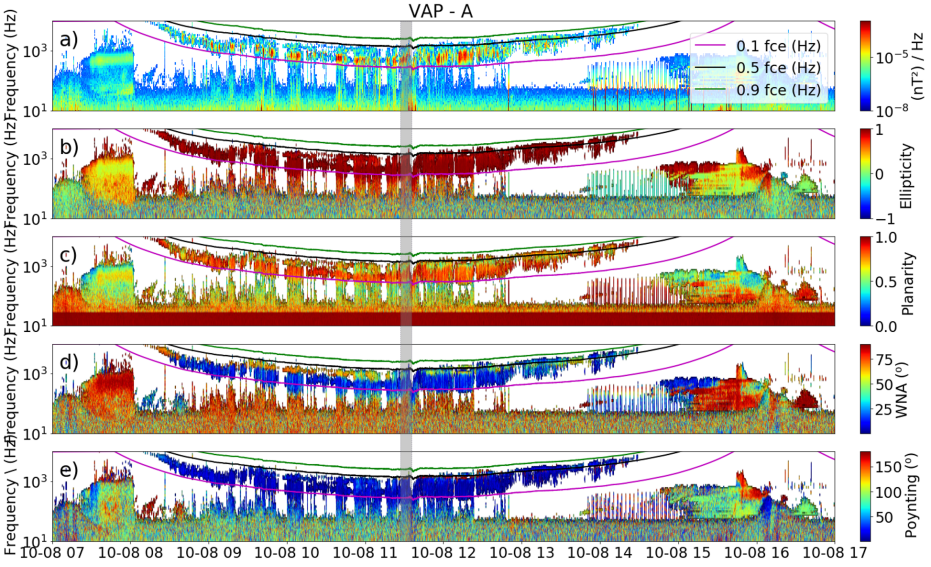

Figure D1. Panels from 08 October 2012, Case 1, show the whistler-mode chorus waves (a) spectrum of the magnetic field, (b) ellipticity; (c) planarity; (d) WNA – wave Normal angle; (e) the polar angle of Poynting vector. In all panels, the t values of 0.1fce (Hz), 0.5fce (Hz), and 0.9 fce (Hz) are shown by the pink, black, and green lines, respectively. The parameters shown from the gray shaded period are used to calculate the time of interaction and change in pitch angle for the resonant electrons energy shown in table 1.

https://doi.org/10.5194/angeo-2023-6
Preprint. Discussion started: 28 February 2023

Annales Geophysicae Discussions
Open Access
EGU

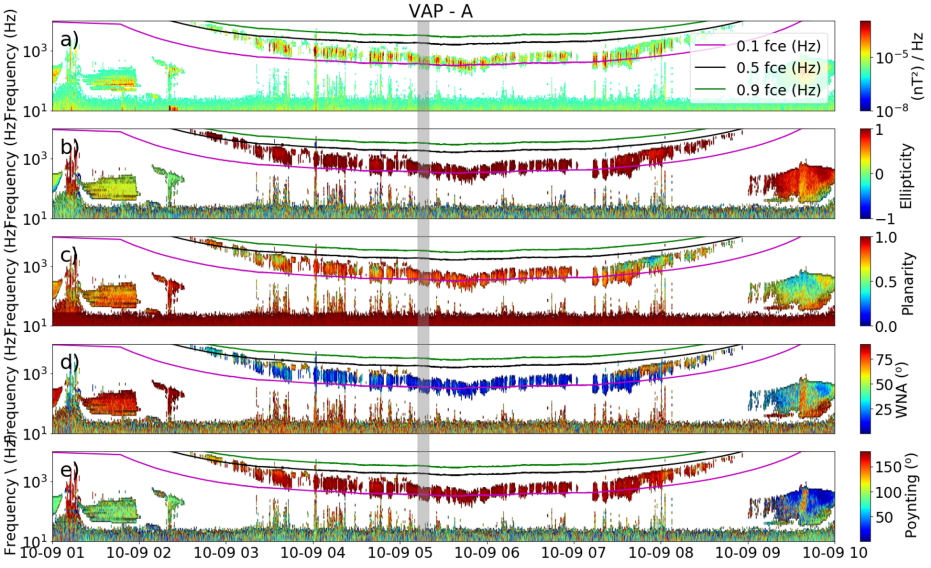

Figure E1. Same as Figure D1 for 09 October 2012, Case 2

https://doi.org/10.5194/angeo-2023-6
Preprint. Discussion started: 28 February 2023

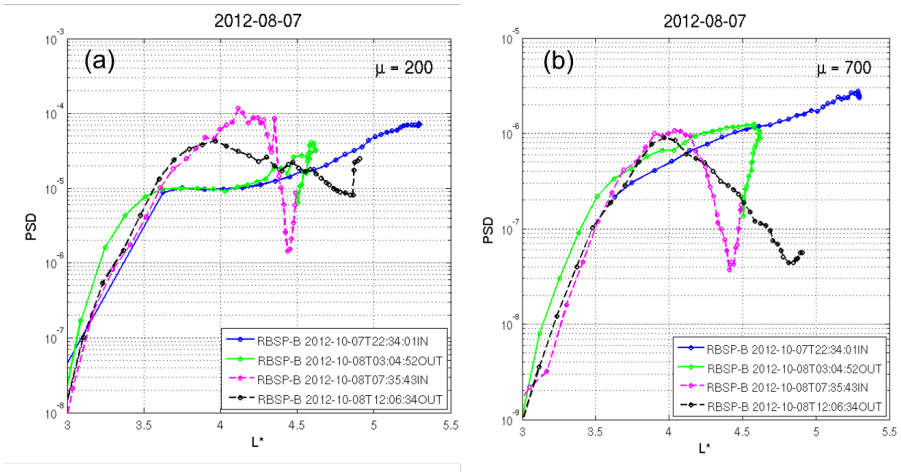

Figure F1. Time evolution of phase space density (PSD) radial profiles at fixed first adiabatic invariant, μ=200MeV/G (a) and μ=200MeV/G (b), and second (K=0.11G1/2RE) adiabatic invariant for both inbound and outbound parts of the RBSP-B orbit. Period of analyses: 07 Oct 2012 at 22:34:01 UT to 08 Oct 2012 at 12:06:34 UT

https://doi.org/10.5194/angeo-2023-6
Preprint. Discussion started: 28 February 2023

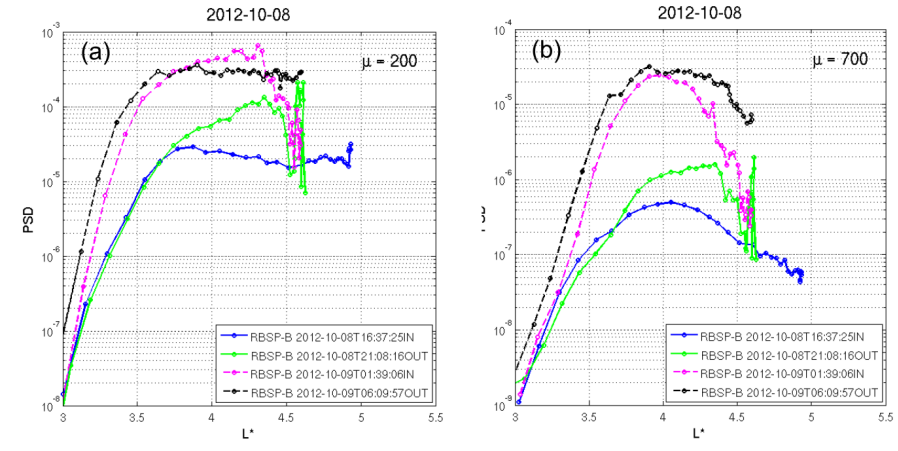

Figure G1. Same as Figure F1 for the period of analyses: 08 Oct 2012 at 16:37:25 UT to 09 Oct 2012 at 06:09:57 UT.